RSC Advances

This is an *Accepted Manuscript*, which has been through the Royal Society of Chemistry peer review process and has been accepted for publication.

Accepted Manuscripts are published online shortly after acceptance, before technical editing, formatting and proof reading. Using this free service, authors can make their results available to the community, in citable form, before we publish the edited article. This *Accepted Manuscript* will be replaced by the edited, formatted and paginated article as soon as this is available.

You can find more information about *Accepted Manuscripts* in the Information for Authors.

Please note that technical editing may introduce minor changes to the text and/or graphics, which may alter content. The journal's standard Terms & Conditions and the Ethical guidelines still apply. In no event shall the Royal Society of Chemistry be held responsible for any errors or omissions in this *Accepted Manuscript* or any consequences arising from the use of any information it contains.

ROYAL SOCIETY OF CHEMISTRY

www.rsc.org/advances

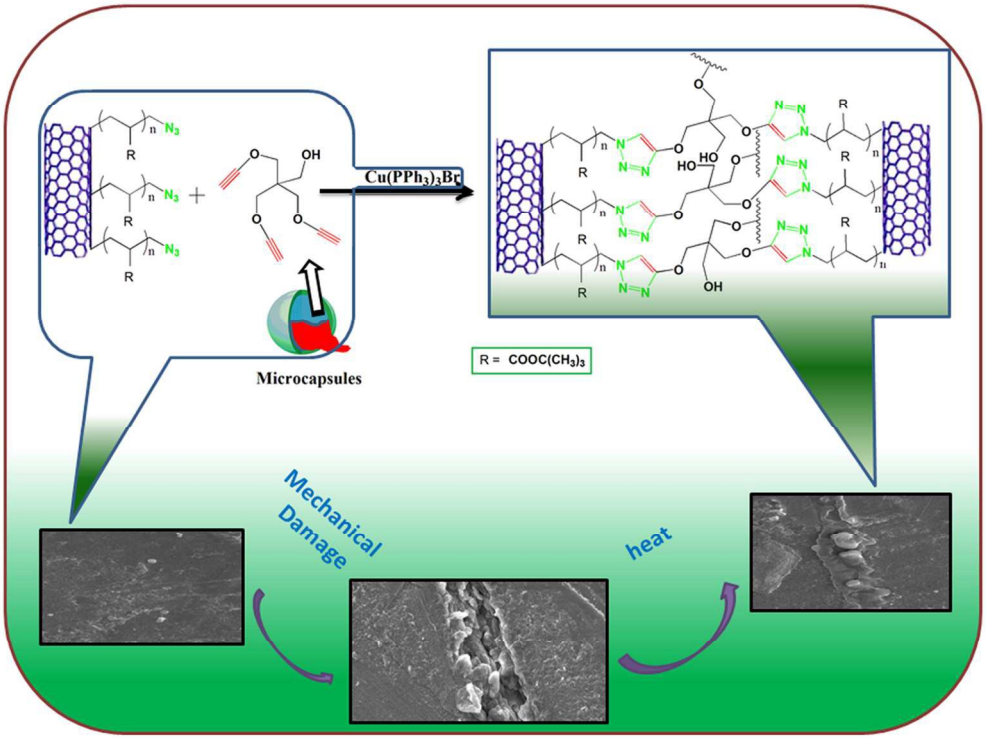

135x101mm (300 x 300 DPI)

RSC Advances Accepted Manuscript

Preparation and characterization of an azide-alkyne cycloaddition based self-healing system via semiencapsulation method

*Bhaskar Jyoti Saikia, Swapan Kumar Dolui**

Corresponding author: swapandolui@gmail.com

Keywords: Self-healing polymer, Urea-formaldehyde Microcapsule, Epoxy resin, ATRP, Click-chemistry.

Abstract:

An azide-alkyne cycloaddition based self-healing system was designed by semiencapsulation method. Multiwall carbon nanotube was functionalized with poly(t-butyl acrylate) containing azide end functionality using atom transfer radical polymerization. Subsequently the alkyne counterpart was encapsulated in urea formaldehyde microcapsules and embedded in an epoxy matrix. The healing click reaction was triggered by an embedded copper catalyst. Whenever a damaging event occurs in the epoxy matrix the liquid cross linker in the presence of catalyst will dissolve the implanted catalyst from the matrix initiating the crosslinking reaction between azide and alkyne and thus healing the cracks. The effects of temperature and healing duration on healing efficiency are investigated. Once healed, the self-healing system recovers as much as 65% of its original fracture toughness.

Introduction:

Inspired by the nature's most astonishing features of self-repairing, the development of self-healing polymeric materials has been a subject on the frontier of research over the last decade[1-3]. Presently, humanity is in an age of plastic. Polymers and their composites are used in almost

RSC Advances Accepted Manuscript

every material used by modern society. However, these materials are susceptible to damage which may be induced by mechanical, chemical, UV radiation, thermal, or any combination of these factors[4]. Whenever these polymeric materials damaged, only a few methods are available to extend their service life. However, majority of structural failure results from the propagation of initial microcracks. Eventually if repairing can be made at the micro level, the lifetime of the materials can be significantly enhanced. Encapsulation of monomers/catalysts into polymer matrix, dynamic covalent bond formation and supramolecular self-assembly are the prevalent adopted strategies for preparing self-healing polymers[5-12]. Among various approaches investigated, atom transfer radical polymerization (ATRP) and click chemistry are the most versatile means for tailoring the functionality of a polymer towards development of effective self-healing systems.[13-17]

Preparation of multifunctional and well-defined macromolecules requires a smart selection of controlled polymerization (CRP) technique in combination with appropriate coupling reactions. ATRP is the most versatile CRP method owing to its exceptional properties like preparation of polymer with predetermined molecular weight, narrow polydispersity index, predetermined chain end functionality and tunable architecture[18-20]. Click chemistry is a powerful coupling approach which in combination with ATRP can be used for generation of polymers having almost all of the desired properties.[21-25]

Click chemistry has been extensively used as a crosslinking reaction while designing self-healing polymers providing high healing efficiency. Among these reactions the Huisgen 1,3-dipolar cycloaddition reaction of organic azides and alkynes also known as CuAAC has gained

RSC Advances Accepted Manuscript

considerable attention as they are very robust, simple, insensitive and can be used as a polymerization reaction for synthesis of long linear polymers.[26-29]

Recently, a number of metal chelating systems based on 1, 2, 3-triazoles and various 1, 2, 3-triazole containing ligands synthesized by CuAAC has been employed successfully for designing self-healing systems[30-33]. However, most of the systems are gels, lacking mechanical and thermal stability for structural applications and requires the presence of suitable metal ions. In this report, we have designed an efficient self-healing system based on direct CuAAC via semi encapsulation approach which has the flexibility of choosing any matrix and enjoy reinforcement by MWCNT. The main strategy for a semi capsulation method is that a matrix is prepared with either inherent or implanted azide (or alkyne) functionality with embedded copper catalyst (preferably $CuBr(PPh_3)_3$) and microcapsules containing the compliment functionality alkyne (or azide). As soon as the damaging event occurs the liquid cross linker in presence of catalyst embedded in the matrix will initiate the crosslinking reaction between azide and alkyne and thus healing the cracks. For this purpose, we have first functionalized multiwall carbon nanotube (MWCNT) with ATRP initiator then functionalized with poly (t-butyl acrylate). The bromine end group was subsequently converted to azide and used as multifunctional azide which acts both as crosslinker and provides reinforcement. Urea-formaldehyde microcapsules containing tripropargylpentaerythritol was synthesized via in-situ condensation method. Finally azide functionalized MWCNT, tripropargylpentaerythritol containing microcapsules and $CuBr(PPh_3)_3$ were embedded into an epoxy matrix to obtain the self-healing composites.

Materials:

RSC Advances Accepted Manuscript

$CuBr_2$ (99.99%, Aldrich), N,N,N',N'',N'' pentamethyldiethylenetriamine (PMDETA) (99% ,Aldrich), pentaerythritol (99%, Sigma-Aldrich), propargyl bromide solution (80 wt. % in toluene), sodium azide(99.99%, Aldrich), epoxy resin (Epoxy equivalent weight:170–180 g/eqiv.) , epoxy hardener [poly(amido amine)] (Kumud Enterprises, Kharagpur, WestBengal, India) and MWCNT(REDEX tech. pvt. ltd) were used as received without further purification. CuBr (98%, Aldrich) was purified by washing with glacial acetic acid, followed by absolute EtOH and Et_2O, and kept under nitrogen after dried under vacuum. t-butyl acrylate (98%, Aldrich) was purified by passing through short basic alumina column. $CuBr(PPh_3)_3$ was prepared following a previously published procedure[34]. All solvents were dried using the standard methods.

Experimental:

Functionalization of MWCNT:

Functionalization of MWCNT with ATRP initiator:

MWCNT was functionalized with ATRP initiator by modification of a previously reported procedure[35]. In a typical procedure 0.5 g MWCNT was charged in a 50 mL round bottom flask containing 20 mL of N-methyl-2-pyrolidinone. The mixture was subjected to sonication for 1h and purged with ultra-high pure nitrogen for 30 minutes. To the reaction vessel 0.3 mmol CuBr and 0.4 mmol PMDETA was added and stirred under continuous nitrogen flow for another 30 minutes to allow the copper complex to form. Finally 0.5 mmol of ethyl α-bromoisobutyrate was injected into the reactor via a degassed syringe and transfer to an oil bath preheated at 70 ^oC. After 48 h functionalized MWCNT was collected via filtration and washed many times with hot water and THF to remove any physically adsorbed reactant until the filtrate showed an absence

RSC Advances Accepted Manuscript

of α-bromoisobutyrate and dried in a vacuum oven at 50 ^{o}C. The % of ethyl α-bromoisobutyrate in **MWCNT-Br** was found to be about 20 weight% from TGA measurement.

Grafting of MWCNT-Br with t-BA:

MWCNT-Br contains bromine end groups which can initiate an ATRP reaction. A graft polymer of t-butyl acrylate was synthesized using the functionalized MWCNTs. **MWCNT-Br** was grinded well in a mortar before proceeding. In a typical procedure 0.3 g powdered **MWCNT-Br** was charged in a three necked round bottom flask containing 10 mL t-butyl acrylate. The mixture was stirred and sonicated alternatively for 45 minutes. It was then kept under continuous nitrogen flow for 15 minutes. 0.50 mmol CuBr and 0.60 mmol PMDETA was added subsequently. Finally polymerization was allowed to occur at 60 ^{o}C under continuous stirring. After 20 h the reaction mixture was poured into excess THF and product was collected by filtration after multiple times washing with hot water. **MWCNT-t-BA** obtained so was dried under vacuum at 50 ^{o}C.

Synthesis of azide end functionalized MWCNT-t-BA:

MWCNT-t-BA contains bromine end group in each chain end which was converted to azide by a simple nucleophilic substitution reaction. Accordingly 0.50 g **MWCNT-t-BA** was dispersed in DMF by ultra-sonication where 2g NaN_3 was added. The mixture was stirred in the room temperature for 48 h. **MWCNT-t-BA-N_3** obtained so was collected by filtration after washing with hot water for several times.

Synthesis of tripropargylpentaerythritol:

RSC Advances Accepted Manuscript

For synthesis of tripropargylpentaerythritol, 5g pentaerythritol was dissolved in 50 mL DMSO and placed in an ice bath. 30 mL triethylamine was added to the above mixture and stirred for 30 minutes. Then 20 mL propargyl bromide mixed with 10 mL DMSO was added dropwise in 30 minutes via a dropping funnel while keeping the temperature below 5 ^{o}C. It was then allowed to stir in room temperature for another 48 h. Finally the mixture was poured into 100 ml diethyl ether and washed with distilled water (50mLx3) to remove any unreacted pentaerythritol. The organic phase was then dried over anhydrous $MgSO_4$ while solvent was evaporated in a rotary-evaporator. The crude product obtained was purified via column chromatography using hexane/diethyl ether 1:1 yielding 3.9 g of pale yellow viscous liquid.

Synthesis of urea formaldehyde microcapsules containing Tripropargylpentaerythritol:

Preparation of Pre-polymer:

37% formaldehyde (0.1 mol) and urea (0.05 mol) were added to 20mL distilled water in a 250 mL three-necked round bottom flask equipped with a reflux condenser and magnetic stirring bar. pH of the mixture was adjusted to ~8 by dropwise addition of triethylamine. It was then transferred to an oil bath preheated to 70 ^{o}C and stirred for 1 h. Completion of the reaction was monitored by adding a drop of reaction mixture to water and examining for turbidity. Reaction was stopped as soon as turbidity appears.

Emulsion preparation

A solution of 0.8 g SDBS in 70 mL distilled water was prepared and 10 mL 1% (W/V) PVA was added to it. 8mL of tripropargylpentaerythritol was added to the above solution dropwise in 30 minutes and stirred at a rate of 1200 rpm for additional 1 h to get stable oil in water emulsion.

RSC Advances Accepted Manuscript

Synthesis of microcapsules:

The rate of stirring of above emulsion was reduced to 500rpm while prepolymer solution was added to it slowly. The temperature was raised to 70 ^{o}C and simultaneously pH was lowered slowly to ~4 in three steps at an interval of 15 minutes. 1% formic acid was used for pH adjustment. The micro-capsulation process was continued for additional 1h at the final pH. Finally the reaction mixture was cooled to room temperature and resultant slurry was neutralized by adding 10% $NaHCO_3$ solution. Microcapsules were rinsed many times with water and acetone and finally filtered and air dried.

Preparation of epoxy composites containing Tripropargylpentaerythritol-loaded microcapsules and MWCNT-t-BA-N_3 / CuBr $(PPh_3)_3$

In a typical process 0.5g **MWCNT-t-BA-N_3** and 0.1g CuBr $(PPh_3)_3$ (0.5%) was ultrasonicated in 30 mL acetone and 25g epoxy resin was added to it. The mixture was further sonicated and stirred alternatively for 1h and transferred to a round bottom flask equipped with a mechanical stirrer. 5 g microcapsule was added to the mixture under vigorous stirring. Acetone was then evaporated by heating the mixture under stirring. After 2h of stirring 25 g hardener was added and stirred for additional 15 minutes. The viscous mass was finally transferred to molds and allowed to crosslink in the room temperature for 24h and 100 ^{o}C for another 24h.

Instruments and methods:

^{1}H NMR was measured by JEOL 400 MHz NMR instrument using $CDCl_3$ as solvent. The surface structure of the microcapsules as well as the composite particles was determined by SEM (Jeol–JSM–6390LV) coupled with energy dispersive X-ray detector. Composite samples were

RSC Advances Accepted Manuscript

sputter coated with platinum thickness of 200Å.The voltage and working distance was varied during the measurement. Thermo gravimetric analysis (TGA) of composites was studied in a Shimadzu TA50 thermal analyzer. A pre weighted amount of the samples was loaded in a platinum pan while heating was done under nitrogen atmosphere at a heating rate of 5 °C/min in the range of 30-600 °C. FTIR spectra of the hydrogels were recorded with a Nicolet Impact-410 IR spectrometer (USA) in KBr medium at room temperature in the range of 4000–400 cm^{-1}.

Results and discussion:

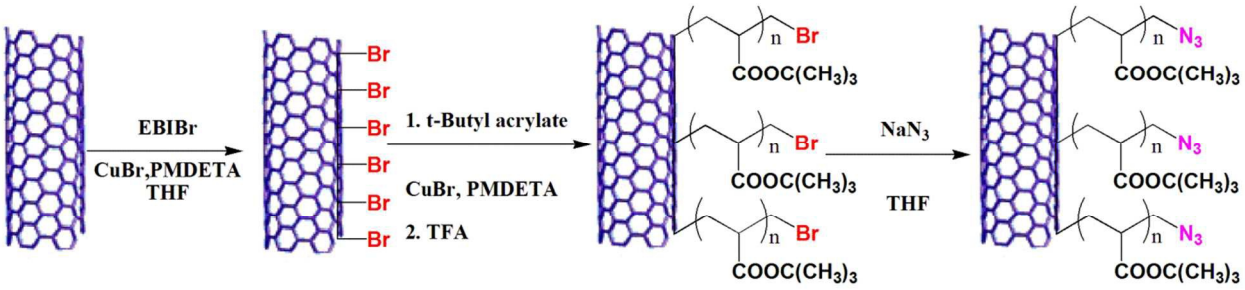

Scheme 1: A schematic representation of functionalization process of MWCNT

MWCNT was successfully functionalized with ATRP initiator and subsequently t-BA was grafted on it. A schematic representation of the process is shown in Scheme 1. Ethyl α-bromo isobutyrate was allowed to undergo ATRP with the double bonds of MWCNT using CuBr/PMDETA catalyst system. The process will result in transfer of bromine atom and hence covalent attachment of ATRP initiator to the MWCNT.

RSC Advances Accepted Manuscript

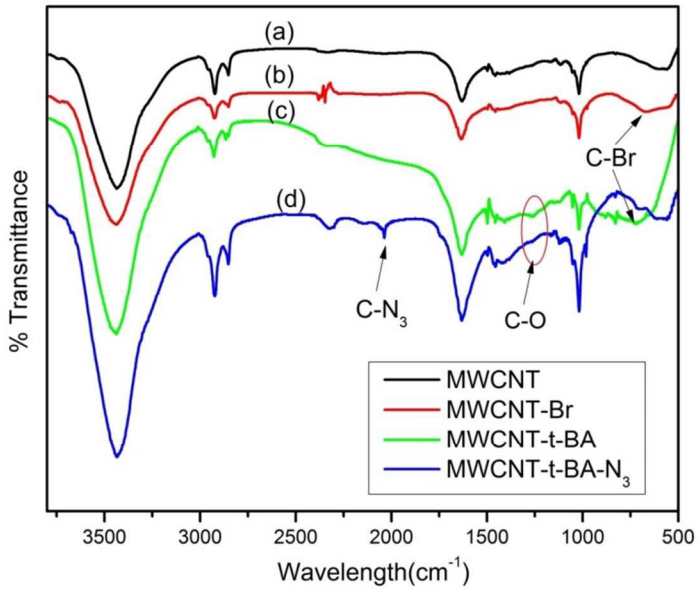

Figure 1: FTIR spectra of (a) MWCNT, (b) MWCNT-Br, (c) MWCNT-t-BA and (d) MWCNT-t-BA-N_3

The attachment of ATRP initiator to MWCNT was confirmed by observing the FTIR spectrum of MWCNT-Br with the absorption peaks at 664 cm^{-1} corresponding to C-Br stretching frequency (Figure 1). The tertiary center so generated on the surface of MWCNT was used for grafting of t-butyl acrylate using same catalyst system. ^{1}H NMR spectra of the MWCNT-t-BA in $CDCl_3$ shows the presence of characteristic peaks at δ =4.52 ppm (>C**H**-Br), 1.92.-2.56 ppm (-C**H**$_2$CH(COOC(CH$_3$)$_3$)-Br), 1.61-1.83 ppm (>C**H**COO(CH$_3$)$_3$) ppm, 1.48 ppm (-C**H**$_2$-), and 1.39 ppm (-C(C**H**$_3$)$_3$) confirming successful formation of t-BA brushes on MWCNT with bromine end group intact. The broader signals in the spectrum of MWCNT-t-BA may be due to local field effects due to MWCNT itself, or slow tumbling of the large polymer brush in solution[36]. (Figure 2)

RSC Advances Accepted Manuscript

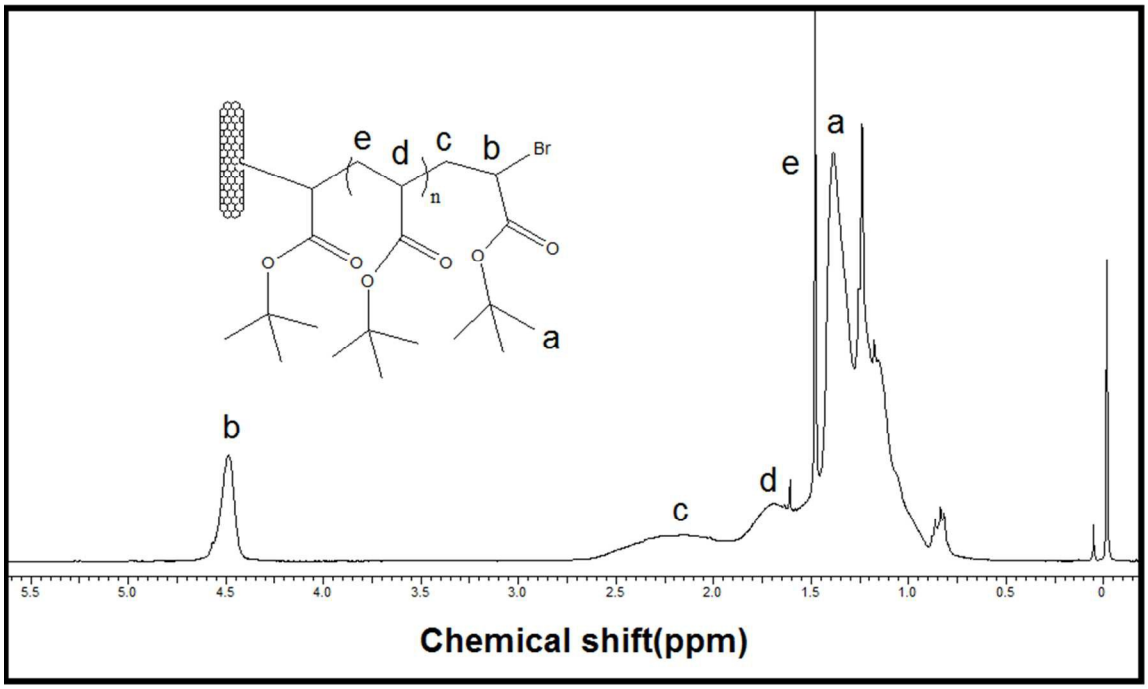

Figure 2: ^{1}H NMR spectra of **MWCNT-t-BA** in $CDCl_3$

Finally the bromine end group of MWCNT-t-BA was converted to azide by treatment with NaN_3. It is seen that in the FTIR spectra of the azide modified polymer new absorption peaks appears at 2037 cm^{-1} corresponding to the $-N_3$ stretching confirming successful conversion of bromide to azide. Presence of C-O stretching frequency in **MWCNT-t-BA** and **MWCNT-t-BA-N_3** at 1249 cm^{-1} further confirms the presence of $-COO(CH_3)_3$. However other characteristic absorption peaks are not distinguishable due to highly absorbing media of MWCNTs. To confirm that **MWCNT-t-BA** was only formed due to EiBr covalently anchored on the MWCNT surfaces, a control experiment was also done using pristine MWCNTs to replace **MWCNT-Br** in the t-BA grafting system. After 36 h, the collected MWCNTs were subjected to TGA measurement which reveals no major weight loss. These results demonstrates that EiBr was successfully attached onto MWCNT surfaces and have the ability to serve as initiating sites for surface-initiating ATRP.

RSC Advances Accepted Manuscript

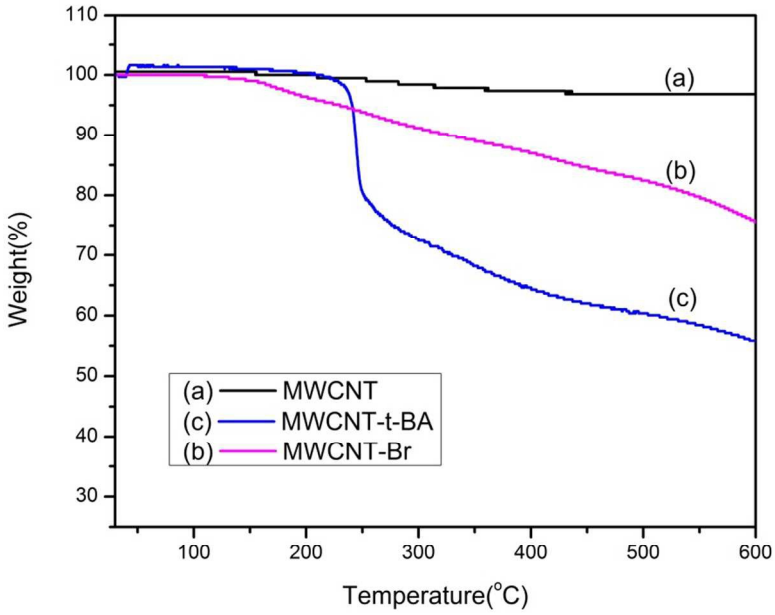

Figure 3: TGA thermogram of (a) **MWCNT** (b) **MWCNT-Br** (c) **MWCNT-t-BA**

Figure 3 represents the TGA thermogram of pristine MWCNT, **MWCNT-Br** and **MWCNT-t-BA**. It is seen that pristine MWCNT shows only 4% degradation while **MWCNT-Br** undergoes 24% degradation till 600 ^{o}C. The degradation of **MWCNT-Br** starts at 157 ^{o}C which originates from the degradation of ethyl isobutyrate and bromide covalently attached to MWCNT. The TGA curve of **MWCNT-t-BA** shows a multi-step weight loss. Degradation starts at 230 ^{o}C and nearly half of the total degradation occur at that temperature. There is also some weight loss at 260 and 420 °C which contribute the remaining half of the total degradation. The degradation pattern corresponds to degradation of poly (t-butyl acrylate) which indicates successful grafting of t-BA from **MWCNT-Br** surface.

RSC Advances Accepted Manuscript

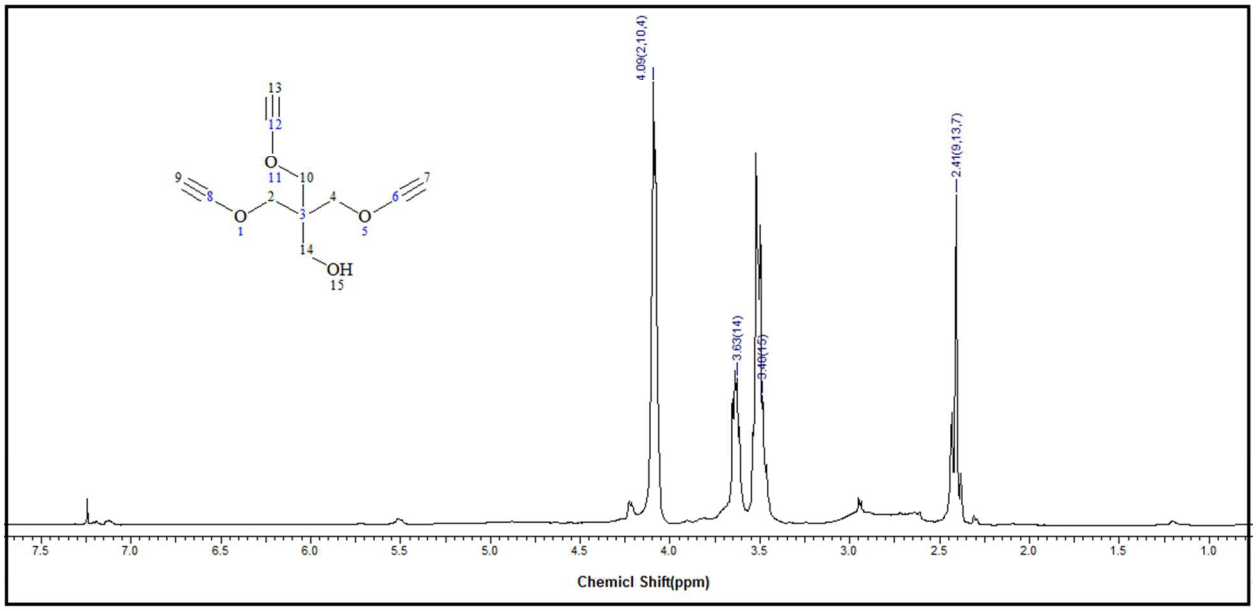

Figure 4: ^{1}H NMR spectra of tripropargylpentaerythritol in $CDCl_3$.

The healing liquid for microcapsules tripropargylpentaerythritol was synthesized by simple nucleophilic substitution reaction of pentaerythritol with propargyl bromide. The structure was established by ^{1}H NMR spectroscopy with characteristic chemical shift values at $\delta = 4.09$ ppm (-C**H**$_2$-O), 3.63 ppm (-C**H**$_2$-OH), 3.40ppm (-O**H**), 2.41 (≡C-**H**). (Figure 4)

RSC Advances Accepted Manuscript

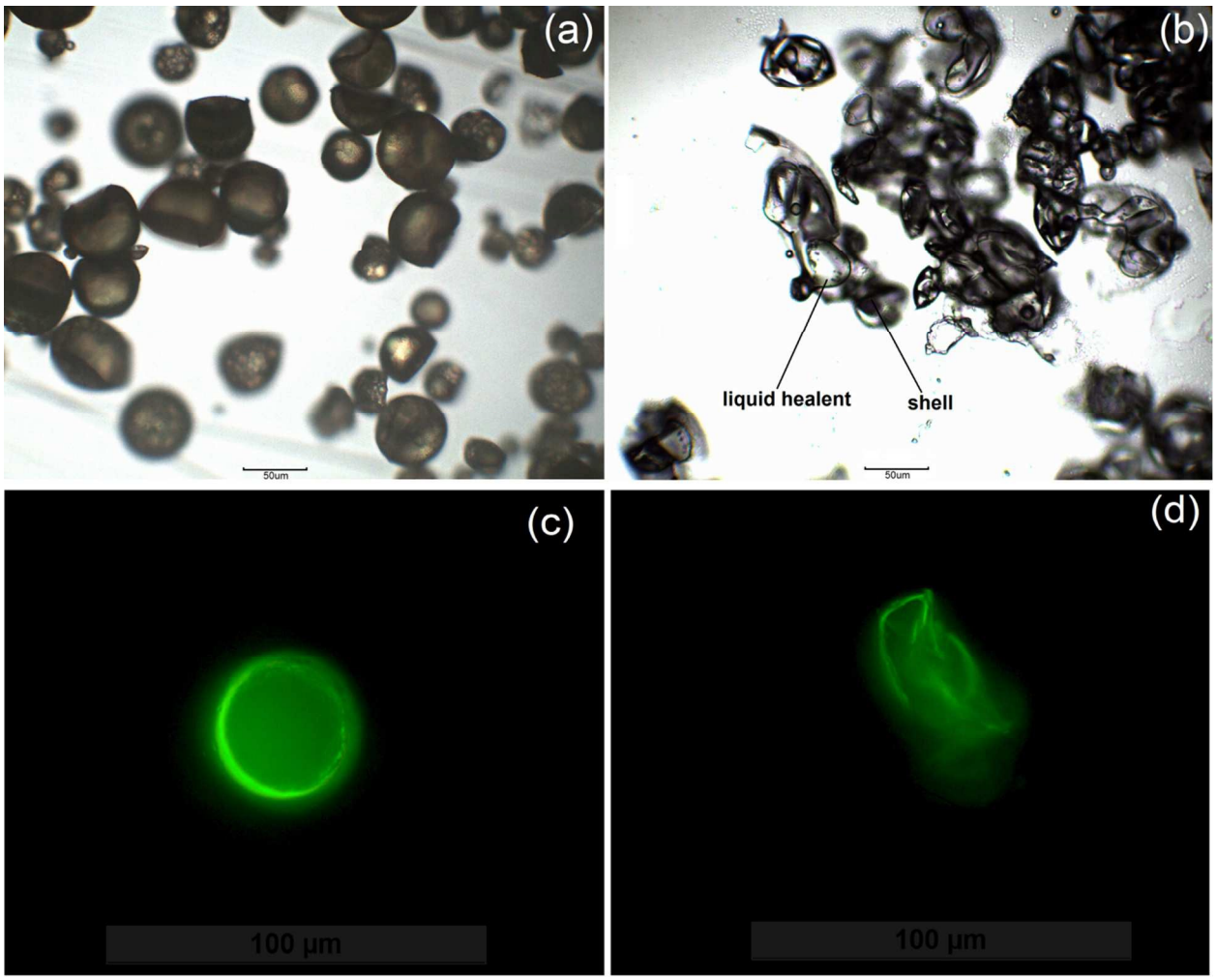

Figure 5: Figure (a) and (b) represents the optical microscope image of UF microcapsules between two glass slides before and after compression and figure (c) and (d) represents corresponding fluorescence microscopy images.

The urea formaldehyde microcapsules containing tripropargylpentaerythritol were prepared via in-situ condensation method. The controlling parameters were used following literature procedure reported by Zhang Ting et. al[37]. Initially the encapsulation process was monitored by an optical microscope. Figure 5.a shows the optical microscope image of prepared microcapsules. Almost all the microcapsules were found to be of spherical shape. In the optical

RSC Advances Accepted Manuscript

microscopy study of the microcapsules we found the appearance of diffraction rings which is in accordance with the theory of optics indicating successful incorporation of healing liquid inside.[38] Optical microscope image of the glass slides compressed microcapsules in figure 5.b clearly shows the bleeding of the healent out of the capsules. To further confirm the encapsulation of the healing liquid inside the microcapsules 10-styrylanthracene was mixed with tripropargylpentaerythritol before encapsulation and was observed with fluorescent optical microscope. Green bright fluorescent microcapsules in figure 5.c and corresponding broken microcapsule 5.d confirms the successful incorporation of the healent inside UF shells.

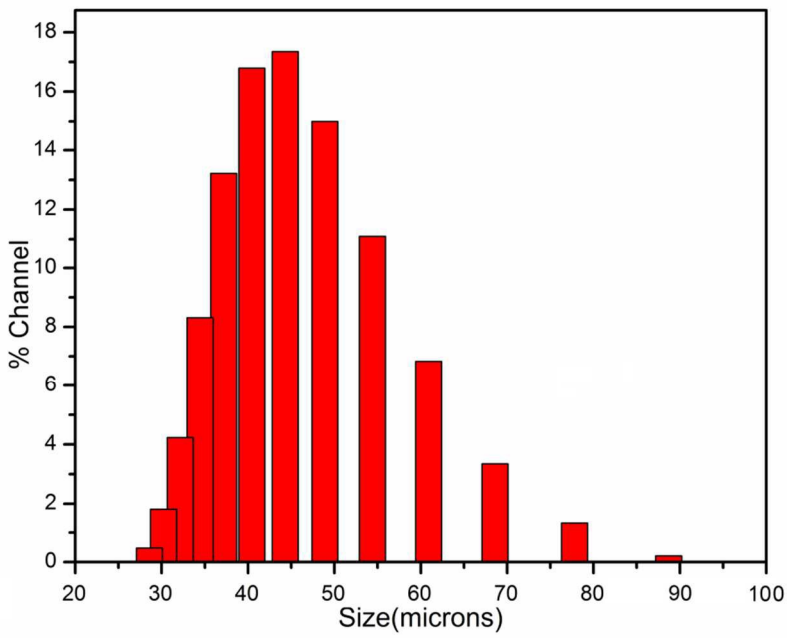

Figure 6: Size distribution histogram of the prepared microcapsules.

The size distribution histogram of the prepared microcapsules is shown in the figure 6 Microcapsule size was found to be in a wide range 25-90 μm. It may be due to the fact that the fluid flow around the propeller is turbulent, in the region of flow away from the propeller, many larger microeddies exist, and in the vicinity of the propeller blades, many smaller microeddies

RSC Advances Accepted Manuscript

exist, which result in a wider distribution of capsule size. In our case the mean diameter of the prepared microcapsules is found to be ~45µm which is quite satisfactory for the use in self-healing of material.

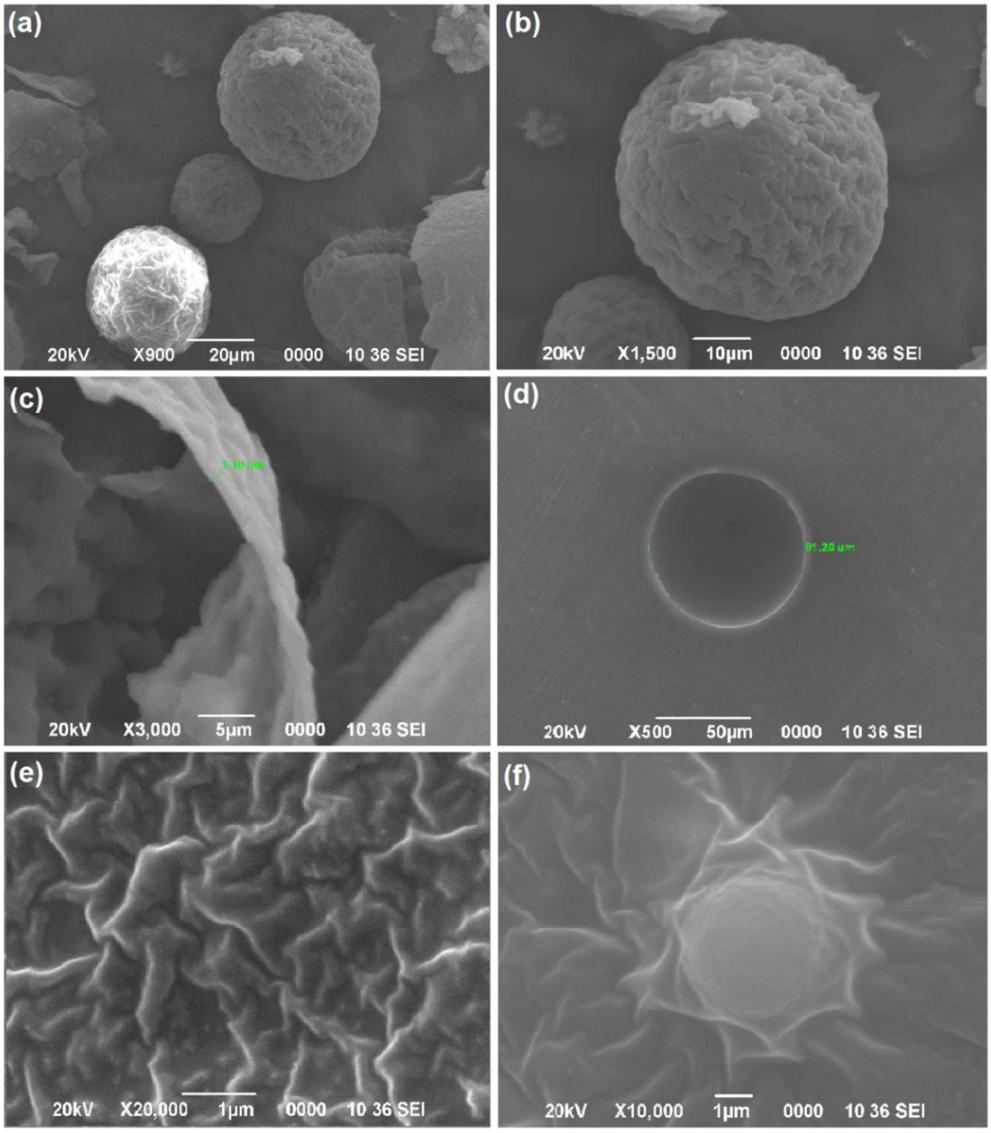

Figure 7: SEM micrograph of UF microcapsules (a) & (b), wall of the microcapsules (c), fracture surface of the composite (d), **MWCNT-t-BA-N_3** in the composite (e), a microcapsule on the surface of the composite.

RSC Advances Accepted Manuscript

Surface morphology and size of the microcapsules were determined by SEM micrograph. Figure 7 shows the SEM micrograph of microcapsules. It is clear from the micrograph that surface of microcapsules are rough which may be due to presence of UF nanoparticles protruding from the surface. The protuberant nanoparticle enhances the surface area of microcapsules offering better surface adhesion. The microcapsules were found to be spherical with average diameter of about 50 μm. Thickness of shell wall of microcapsules mainly depends on the manufacturing parameter which in turn determines the mechanical property of the microcapsules. Figure 7(c) shows the wall thickness of a cracked microcapsule and figure 7(d) shows the SEM image of a microcapsule in a cross-section of prepared composite. In our study the wall thickness of the synthesized microcapsules were found to be 1.1 μm. The microcapsules are clearly visible in the matrix (figure 6(f)) which indicates that embedded microcapsules still maintain their integrity and are well adhered to the matrix without undergoing any damage during processing conditions. The inner surface of the microcapsule formed was found to be smooth and compact which allows easy flow of healing agent into the crack. SEM micrograph shows uniform dispersion of MWCNT-N_3 in epoxy resin with few small remaining aggregates which are smeared out and well penetrated by the epoxy resin matrix. (Figure 7(e))

RSC Advances Accepted Manuscript

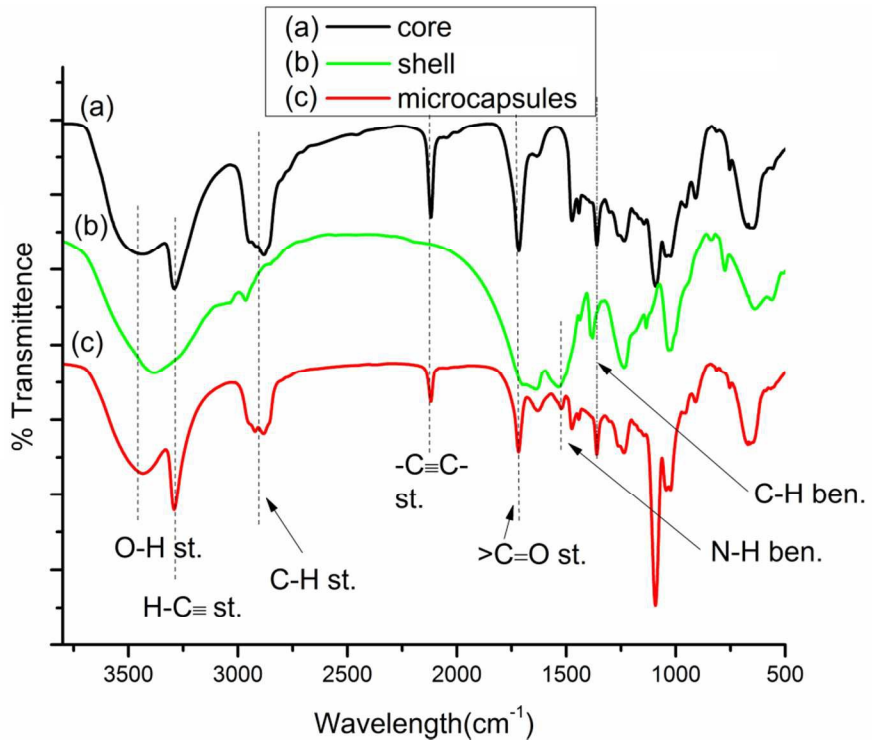

Figure 8: FTIR spectra of tripropargylpentaerythritol (a), UF prepolymer (b) and UF microcapsules(c).

Figure 8(a) represents the FTIR spectra of the core material tripropargylpentaerythritol. The characteristic peaks includes 1715 cm^{-1}, 2118 cm^{-1}, 3286cm^{-1} and 3450 cm^{-1} corresponding to >C=O, -C≡C-, H-C≡ and -OH respectively. Figure 8(b) represents characteristic absorption bands appear due to empty UF polymeric shells. The absorption peak appeared at 3381 cm^{-1} peak denotes –NH and -OH stretching. The stretching frequency at 1531 cm^{-1} corresponds to the N-H banding, 1374 cm^{-1} corresponding to C–H bending and a 1025 cm^{-1} stretching frequency was noted for -CO-NH. Figure 8(c) represents the FTIR spectra for the tripropargylpentaerythritol loaded UF microcapsules which contains all the characteristic absorption peaks for both the core and shell materials confirming successful encapsulation.

RSC Advances Accepted Manuscript

Core content of the microcapsules were determined by solvent extraction. For this purpose some pre-weighted microcapsules were grinded in a mortar to crush it completely. It was then collected and washed with acetone several times to remove any core material. Finally the crushed microcapsules were collected and dried to constant weight. If the initial weight of the microcapsules is W_i and weight of the residual shell wall is W_f then % core content of the microcapsules (C_W) can be given by:

$$C_W = \frac{Wi - W_f}{W_i} \text{ x } 100\ \%$$

Following this procedure the core content of the microcapsules was found to be 78%.

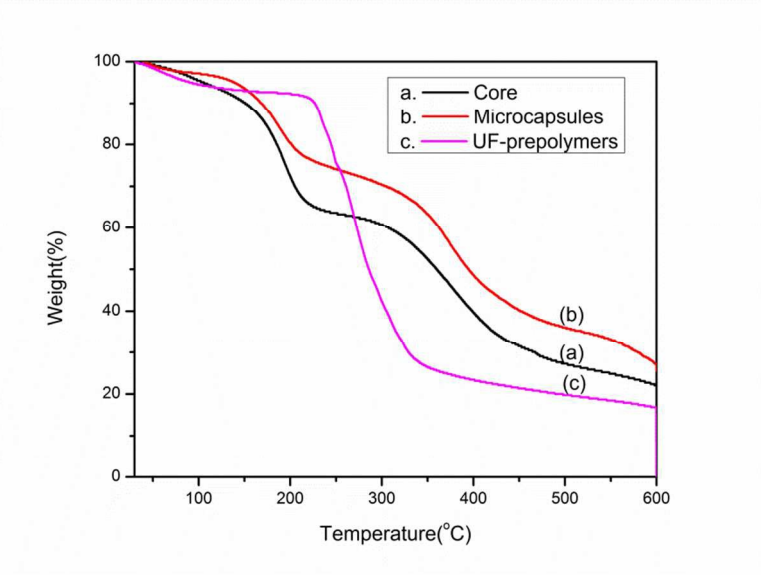

Figure 9: TGA thermogram of (a) tripropargylpentaerythritol, (b) Microcapsules and (c) UF-prepolymer.

Thermal stability of microcapsules plays an important role in their applications as self-healing composite. Figure 9 shows the TGA thermogram of core material, poly urea formaldehyde

RSC Advances Accepted Manuscript

prepolymer and corresponding microcapsules. In the degradation pattern of UF-prepolymer, the weight loss below 200 °C is attributed to the gasification of small molecules such as water, formaldehyde and low molecular weight polymer. Major weight loss observed between 200 and 375 °C is attributed to the pyrolysis of the UF resin. Thermal degradation pattern of tripropargylpentaerythritol exhibits two step degradation patterns. First major weight loss occurs between 150-250 °C and second one occurs at 270-500 °C temperature range. Any weight loss below these temperatures is due to evaporation of water. As for the microcapsules, the weight loss below 150 °C is again attributed to the evaporation of adsorbed water and free formaldehyde. The degradation pattern almost resembles the degradation pattern of the core content of the microcapsules. The thermal stability of the microcapsules are slightly higher than the core material owing to the protection of the shield of the urea–formaldehyde wall. However thermogravimetric study resolves that the microcapsules are stable upto 150 ^{o}C only i.e. the thermostability of the microcapsules is considerably lower than the shell material which can be attributed to the lower thermal stability of the core material.

Tensile strength of neat cross-linked epoxy resins and that containing MWCNT-Br, catalyst and microcapsules were measured in accordance with ASTM-D3039 to access the inclusion of the ingredients. Zwik Roll (10KN) universal testing machine was used at a crosshead speed of 10mm/min in room temperature. Three samples were tested in each case.

RSC Advances Accepted Manuscript

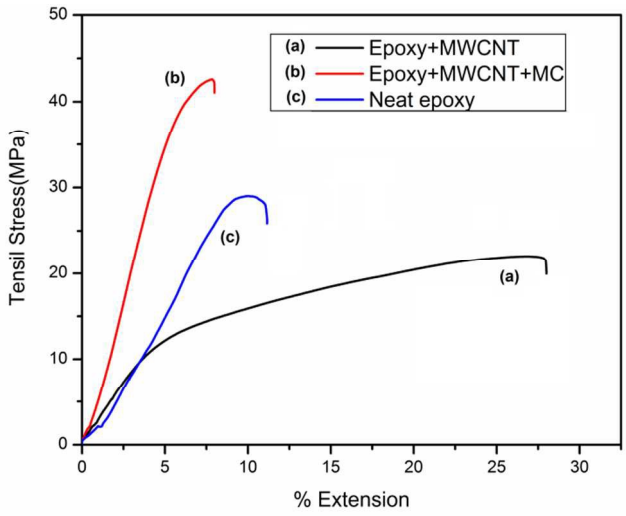

Figure 10: Stress-strain curve for (a) epoxy+ MWCNT, (b) epoxy+ MWCNT+ microcapsules, (c) Neat epoxy.(here MWCNT represents MWCNT-t-BA)

Figure 10 shows the stress–strain curves of the tested samples of neat epoxy, epoxy loaded with **MWCNT-t-BA-N_3** and epoxy loaded with microcapsule, **MWCNT-t-BA-N_3** and catalyst. It was found that ultimate tensile strength and Young's modulus of the epoxy decreases on addition of functionalized MWCNT while flexibility increases substantially. This occurs due to inhomogeneous distribution of MWCNT and slippage of graphite layers of MWCNT. After incorporation of all the ingredients the ultimate tensile strength and Young's modulus increases substantially compared to the neat epoxy while elasticity decreases. It is due to the fact that shell material of the microcapsules i.e. urea–formaldehyde resin, is compatible with epoxy and considerably strong interfacial interaction occurs during curing. Although at high concentration of MWCNT homogenous dispersion is not possible which tend to decrease the tensile strength but at the same time the microcapsule hard walls are able to withstand some load transferred by the interface.

RSC Advances Accepted Manuscript

Single-edge notched bending (SENB) test was performed to measure plane-strain fracture toughness and hence to evaluate self-healing ability of the prepared composites. In accordance with ASTM standard D5045-99, prior to testing a notch was precasted and then sharpened by tapping a fresh razor blade into the material. Three samples were tested in each condition. A loading rate of 10 mm/min was applied for the test. The original specimens were tested to failure, giving the fracture toughness, K^0_{IC}. It was then clamped together and heated in an oven at preset temperature allowing the healing process to occur. The healed specimens were then retested to yield the fracture toughness, K'_{IC}. Accordingly, the healing efficiency of the prepared epoxy was calculated by using the formula:

$$\eta = K'_{IC} / K^0_{IC} \text{ X } 100\ \%$$

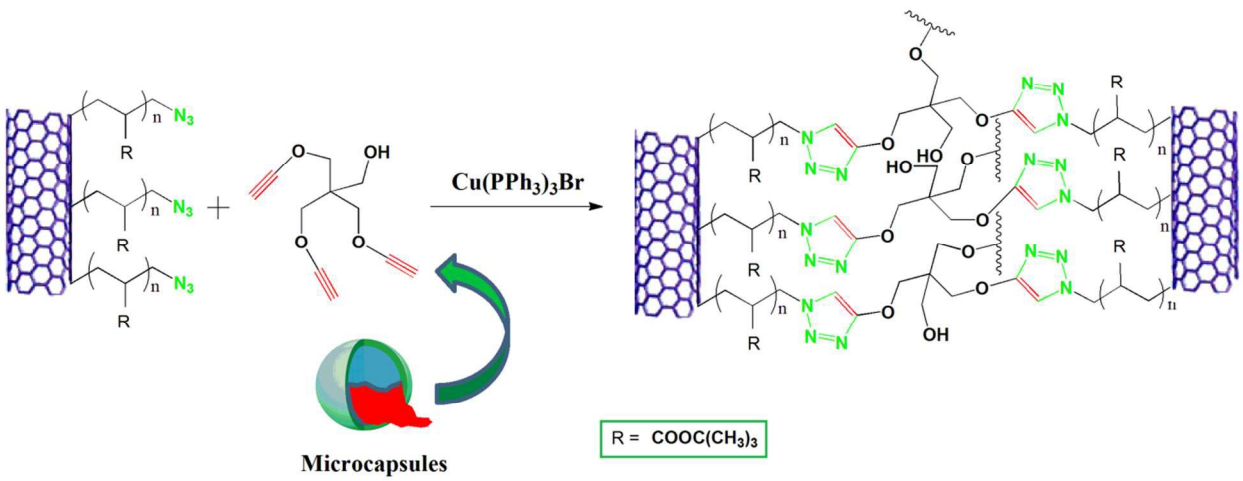

Scheme 2: A schematic representation of the self-healing process.

A schematic representation of the self-healing process is presented in Scheme 2. Azide alkyne cycloaddition between the MWCNT-N_3 in the epoxy matrix and tripropargylpentaerythritol from microcapsules in presence of CuBr $(PPh_3)_3$, as catalyst constitutes the healing mechanism. It can

RSC Advances Accepted Manuscript

be visualized from the SEM micrograph of the composites that rough exterior shell wall of the microcapsules leads to formation of a three-part interphase consisting of thin continuous interior shell wall of the microcapsules, the rough exterior shell wall of the microcapsules and the continuous epoxy matrix. The Epoxy matrix is well penetrated through the rough outside wall of the microcapsules promoting high possibility of capsule fracture, and hence increasing probability of healing agent delivery.

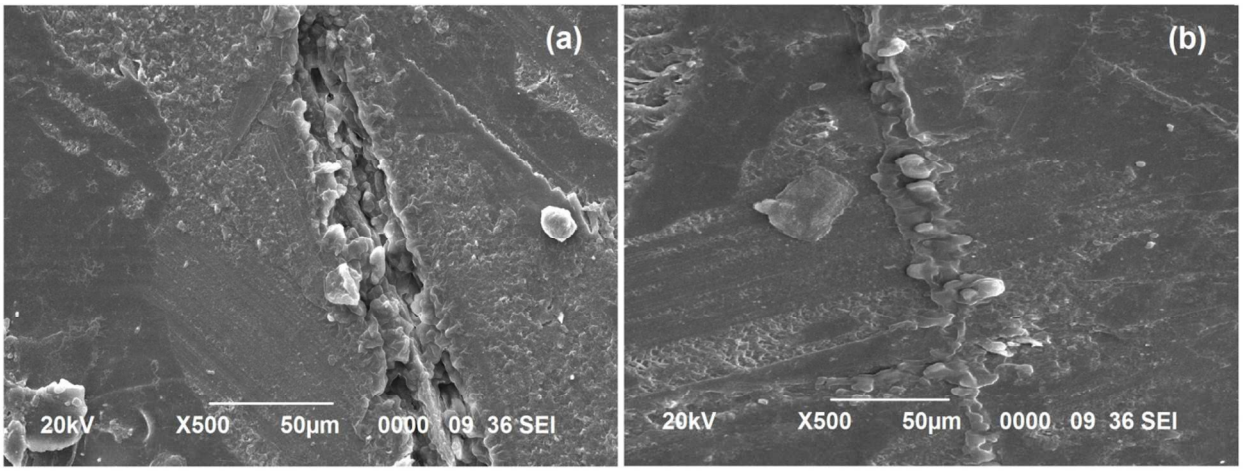

Figure 11: SEM micrograph showing a razor blade pre-notched composite before (a) and after (b) healing.

Figure 11 shows the SEM image of a crack created by a sharp razor blade before and after healing (for 120h at 100 ^{o}C). It is very clear from the figure that a successful healing of the crack was occurred.

RSC Advances Accepted Manuscript

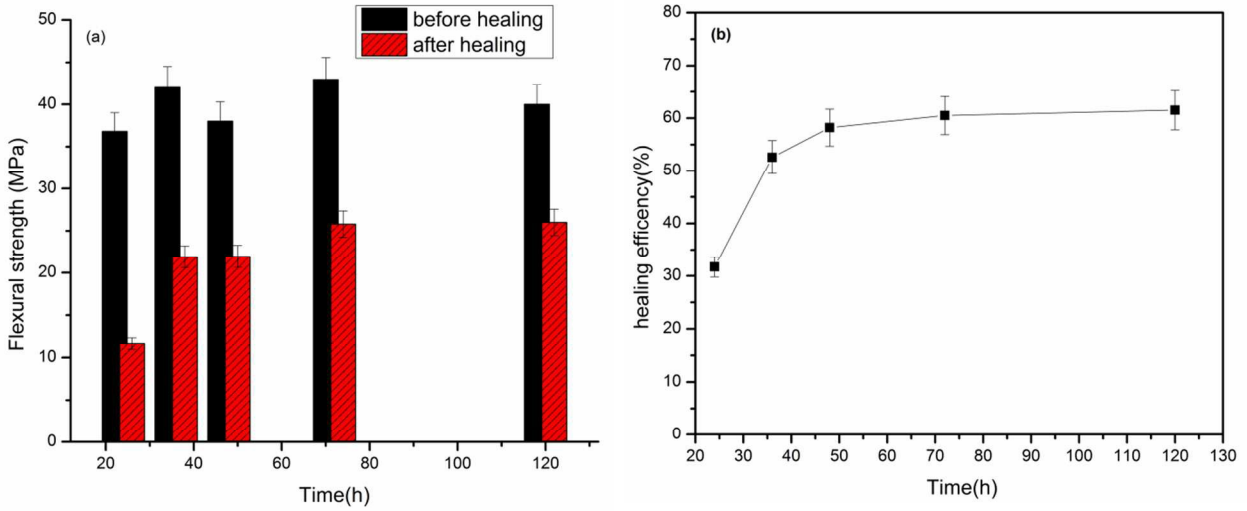

Figure 12: Flexural strength of prepared composites before and after healing at various times (a) and variation of healing efficiency with time at constant temperature of 100 ^{o}C (b).

Primarily crack healing efficiency of the prepared epoxy composite was evaluated for the sample cured up to 100 ^{o}C. Figure.12 shows the fracture toughness of the virgin and cures epoxy resins and variation of healing efficiency with time at constant temperature of 100 ^{o}C. A maximum healing efficiency of 60.2% was obtained upon heating the samples to 120h at this temperature. The healing efficiency shows an exponential increase with time which is due to the fact that more and more healent flow to the crack plane with time. From the fracture toughness measurement it was also found that virgin specimen is less brittle in nature compared to the healed specimen. It may be due to the deformation that occurs during the fracture testing of the virgin specimen which breaks some the microcapsules in the bulk leaching out the crosslinker which undergoes similar reaction as that of healing reaction. This will increase the crosslinking density and hence the brittleness.

RSC Advances Accepted Manuscript

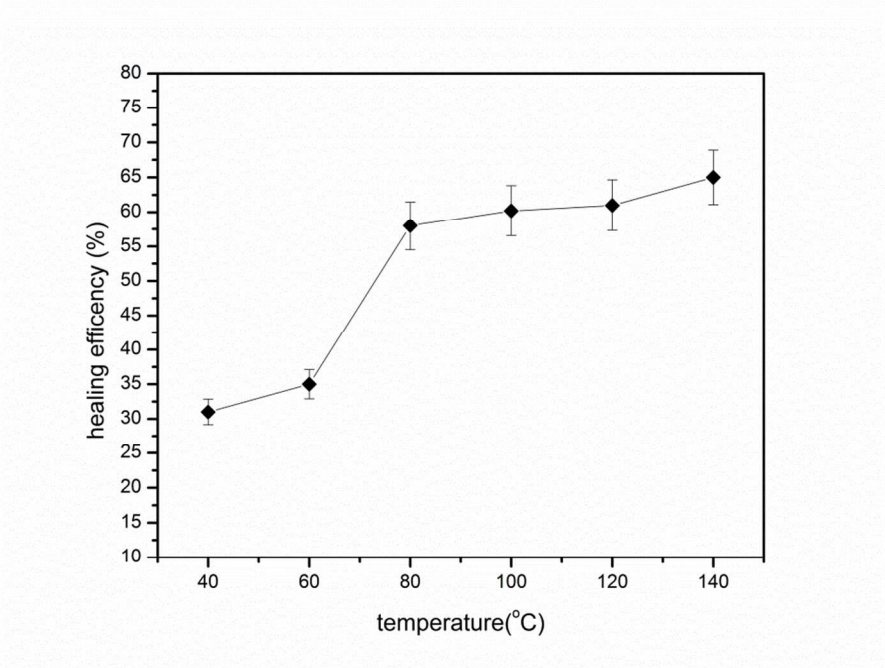

Figure 13: Variation of healing efficiency with temperature with constant heating duration of 120h.

Figure 13 shows the variation of healing efficiency with temperature. All the samples were allowed to heal at various temperatures for a constant amount of time (120h). It is seen that healing efficiency increases with increasing temperature with two remarkable brakes in the curve. Below 60 ^{o}C healing efficiency was very low which increases stripy above this temperature. The healing efficiency between 60-130 ^{o}C shows almost constant behavior. Above this temperature healing efficiency rises again and reaches a maximum of 65 %. This is due to the fact that above 60 ^{o}C the catalyst CuBr $(PPh_3)_3$ drives the azide-alkyne cycloaddition reaction increasing its efficiency. Again above 130 ^{o}C along with copper catalyzed reaction copper free azide alkyne cycloaddition reaction starts to occur which adds to the former to make the healing process more efficient. However further heating above 140 ^{o}C is irrelevant as microcapsules are not stable above this temperature as indicated by TGA thermogram. Although the azide alkyne

RSC Advances Accepted Manuscript

cycloaddition can occur even at room temperature the application of high temperature fastens the healing process not only because of the increasing reaction rate but due to softening the composites bringing the two parts closer. High temperature also helps to solubilize the catalyst and poly(t-butyl acrylate)-N_3 in the liquid crosslinker medium which plays an key role in the healing process.

To evaluate self-healing performance of our system a controlled experiment was performed without the inclusion of microcapsules in the epoxy matrix while enclosing both **MWCNT-t-BA-N_3** and CuBr $(PPh_3)_3$. Samples were broken to failure, clamped together and then heated at 140 ^oC for 120h. However this control experiment showed no healing effects confirming that healing process originates solely due to azide alkyne cycloaddition reaction.

Conclusion:

A well-dispersed azide functionalized MWCNTs/UF-microcapsule/epoxy composites having self-healing ability was successfully fabricated. The UF microcapsules filled with tripropargylpentaerythritol have good storage ability at room temperature and exhibit a good thermal stability below 150 ^oC, which can tolerate the moderate or high temperature processing of polymeric composites. The composite showed a maximum healing efficiency of 65%. Although the healing event occurs at room temperature high efficiency healing was observed at high temperature where uncatalyzed azide-alkyne cycloaddition can also occur along with the catalyzed reactions. In conclusion, this research provides a novel semiencapsulation based self-healing system which can be applied in any polymer matrix requiring this behavior.

RSC Advances Accepted Manuscript

References:

1. X. Chen, M. A. Dam, K. Ono, A. Mal, H. Shen, S. R. Nutt, K. Sheran and F. Wudl, *Science*. 2002, 295, 1698.
2. S. R. White, N. R. Sottos, P. H. Guebelle, M. R. Kessler, S. R. Sriram, E. N. Brown and S. Viswanathan, *Nature*, 2001, 409, 794.
3. X. Chen, F. Wudl, A. Mal, H. Shen, S. R. Nutt and K. Sheran, *Macromolecules,* 2003, 36, 1802.
4. K. Nathalie, K. Guimard, O. Kim, Z. Jiawen, H. Stefan, G. S. Friedrich and B. K. Christopher, *Macromol. Chem. Phys*., 2012, 213, 131.
5. E.N. Brown, N.R. Sottos, S.R. White, *Exp. Mech.,* 2002, 42, 372.
6. M.W. Keller, S.R. White and N.R. Sottos, *Adv. Funct. Mater*, 2007,17, 2399.
7. Z. Guan , J.T. Roland, J.Z. Bai , S.X. Ma, T.M. McIntire and M. Nguyen, *J. Am. Chem. Soc.,* 2004, 126, 2058.
8. R. J. Varley and V. D. Zwaag, *Polym. Test.* 2008, 27, 11.
9. K. Tadano, E. Hirasawa, H. Yamamoto and S. Yano, *Macromolecules*, 1989, 22, 226.
10. P. Zare, M. Mahrova, E. Tojo, A. Stojanovic and W.H. Binder*, J. Polym. Sci. Part A: Polym. Chem.,* 2013, 51, 190.
11. M. Gragert, M. Schunack and W.H. Binder, *Macromol. Rapid Commun.*, 32, 2011, 419.
12. S. Y. An, D. Arunbabu, S. M. Noh, Y. K. Song and J. K. Oh, *Chem. Commun.,* 2015, 51, 13058.
13. T. E. Patten and K. Matyjaszewski, *Adv. Mater.*, 1998, 10, 901.
14. K. Matyjaszewski and N. V. Tsarevsky, *Nature Chemistry*, 2009, 1, 276.
15. K. Matyjaszewski, *Macromolecules,* 2012, 45, 4015.

RSC Advances Accepted Manuscript

16. P. Quirk and J. Kim, *Rubber Chem Technol*. 1991, 64, 450.

17. L. Zhang, W. Liu, L. Lin, D. Chen and M. H. Stenzel, *Biomacromolecules,* 2008, 9, 3321.

18. B. J. Saikia, B. C. Nath, C. Borah and S. K. Dolui, *J. Lumin.*, 2015, doi:10.1016/j.jlumin.2015.07.044,

19. B. J Saikia, D. Das, M. Boruah and S. K. Dolui., *Polym Int.,* 2014, 63, 1047.

20. B. J. Saiki, P. Gogoi, S. Sharmah and S. K. Dolui, *Polym Int.*, 2015, 64, 437.

21. P. Mandal and N. K Singha, *Eur. Polym. J.*, 2015, 67, 21.

22. P. Mandal. and N. K. Singha, *RSC Adv.*, 2014, 4, 5293.

23. L. G. Patricia and K. Matyjaszewski, *QSAR Comb. Sci.,* 2007, 26, 1116.

24. A. J. de Graaf, E. Mastrobattista, C. F. van Nostrum, D. T. S. Rijkers, W. E. Henninka and T. Vermonden, *Chem. Commun.*, 2011,47, 6972.

25. J. F. Lutz , H. G. Börner and K. Weichenhan, *Macromolecules*, 2006, 39, 6376.

26. D. Döhler, P. Michael, and W. H. Binder, *Macromolecules,* 2012, 45, 3335.

27. F. Herbst, S. Seiffertbn and W. H. Binder, *Polym. Chem.*, 2012, 3, 3084.

28. W. Qiang, J. Wang, X. Shen, X. A. Zhang, J. Z. Sun, A. Qin and B. Z. Tang., 2013, *Nature*, Scientific reports 3.

29. S. C. Sukumaran, K. Sunitha, D. Mathew and C. P. R. Nair, 2013, *J. Appl. Polym. Sci.*, 130, 1289.

30. D. Dohler, H. Peterlik and W. H. Binder, 2015, *Polymer*, 69, 264.

31. J. Yuan, X. Fang, L. Zhang, G. Hong, Y. Lin, Q. Zheng, Y. Xu, Y. Ruan, W. Weng, H. Xiaa and G. Chenb, 2012, *J. Mater. Chem*., 22, 11515.

RSC Advances Accepted Manuscript

32. G. Hong, H. Zhang, Y. Lin, Y. Chen, Y. Xu, W. Weng and H. Xia, 2013, *Macromolecules*, 46, 8649.

33. B. Yang, H. Zhang, H. Peng, Y. Xu, B. Wu, W. Weng and L. Liab, 2014, *Polym. Chem.*, 5, 1945.

34. D. V. Allen and and D. Venkataraman, *J. Org. Chem.,* 2003, 68, 4590.

35. Y. L. Liu and W.H. Chen, *Macromolecules*, 2007, 40, 8881.

36. S. Chen, G. Wu, Y. Liu, and D. Long, *Macromolecules.* 2006, 39, 330.

37. Z. Ting, Z. Min, T. Xiao-Mei, C. Feng, and Q. Jian-Hui, *J. Appl. Polym. Sci.,* 2010, 115, 2162.

38. Y. C. Yuan, M. Z. Rong and M. Q. Zhang, *Polymer,* 2008, 49, 2531.

RSC Advances Accepted Manuscript